Vapor-liquid nucleation of argon: Exploration of various intermolecular potentials

Matthew J. McGrath,[1,a)] Julius N. Ghogomu,[2] Narcisse T. Tsona,[2] J. Ilja Siepmann,[3] Bin Chen,[4] Ismo Napari,[1] and Hanna Vehkamäki[1]
[1]*Department of Physics, University of Helsinki, P.O. Box 64, Helsinki FI-00014, Finland*
[2]*Department of Chemistry, University of Dschang, B.P. 67, Cameroon, West Africa*
[3]*Department of Chemistry and Department of Chemical Engineering and Material Science, University of Minnesota, 207 Pleasant Street SE, Minneapolis, Minnesota 55455, USA*
[4]*Department of Chemistry, Louisiana State University, 232 Choppin Hall, Baton Rouge, Louisiana 70803, USA*

(Received 10 April 2010; accepted 12 July 2010; published online 26 August 2010)

The homogeneous vapor-liquid nucleation of argon has been explored at $T=70$ and 90 K using classical nucleation theory, semiempirical density functional theory, and Monte Carlo simulations using the aggregation-volume-bias algorithm with umbrella sampling and histogram-reweighting. In contrast with previous simulation studies, which employed only the Lennard-Jones intermolecular potential, the current studies were carried out using various pair potentials including the Lennard-Jones potential, a modified Buckingham exponential-six potential, the Barker–Fisher–Watts pair potential, and a recent *ab initio* potential developed using the method of effective diameters. It was found that the differences in the free energy of formation of the critical nuclei between the potentials cannot be explained solely in terms of the difference in macroscopic properties of the potentials, which gives a possible reason for the failure of classical nucleation theory. © *2010 American Institute of Physics*. [doi:10.1063/1.3474945]

I. INTRODUCTION

A phase transition is the process by which a new phase is formed from a metastable mother phase. Vapor-liquid nucleation is known to play an important role in the formation of atmospheric aerosols, which affect both human health and climate change, as well as being important in industrial processes.[1] Homogeneous unary vapor-liquid nucleation is one subset of this important genre, involving the condensation of droplets out of a supersaturated one-component vapor phase with no additional seed particles present.

As a result of its importance, the literature surrounding the theory and application of vapor-liquid nucleation is quite extensive; so extensive, in fact, that it is not possible to enumerate it all here. The interested reader is invited to read one of the excellent reviews on the subject (see, for example, the works of Oxtoby,[2] Gunton,[3] the series of articles beginning with Senger *et al.*,[4] or the argon-specific review of Kalilmanov *et al.*[5]). This article will focus only on those techniques that have been applied to the condensation of a monatomic vapor (for example, this means that the significant effort applied to water, alcohols, and alkanes will not be discussed).

Some of the earliest theoretical work in the field was done in 1935 by Becker and Döring,[6] whose efforts signify the beginning of what is termed "classical nucleation theory" (CNT). This is discussed briefly in Sec. II A and in more detail in the reviews listed above. While enjoying relative success in some areas (such as the homogeneous vapor-liquid nucleation of water), failures in others (e.g., *n*-alkanes and argon) have provoked much additional work to be done over the years,[7–16] leading to semiphenomenological approaches,[17–20] dynamical nucleation theory,[21] i/v cluster,[22] n/v cluster,[23,24] n/v-Stillinger cluster method,[4,25] extended modified liquid drop model,[26] mean-field kinetic theory,[27] and various combinations of the above.[28,29]

Another popular approach to studying vapor-liquid nucleation is density functional theory (DFT), which expands the free energy of a system as a functional of the molecular number density. This is sometimes referred to as "nonclassical" nucleation theory, since the capillarity approximation (a fundamental assumption in CNT which states that the physical properties of small clusters are the same as the bulk phases) is not made here. Since the original work of Oxtoby and Evans in 1988,[30] several improvements have been made,[31,32] including dynamical density functional theory,[33] accounting for fluctuations in the system,[34,35] and deriving analytical expressions for the results.[36] Efforts have also been made to approach density functional theory as a semiempirical method; that is, one adjusts some parameters in the theory to reproduce known macroscopic properties of the fluid and then uses these parameters for nucleation calculations.[37,38]

With regard to molecular simulation of vapor-liquid nucleation, both molecular dynamics and Monte Carlo techniques have enjoyed wide usage in the literature. Molecular dynamics simulations have the advantage of being able to closely reproduce the physical process and calculate nucleation rates. Unfortunately, direct nucleation simulations are limited to relatively high supersaturations (low free energy

[a)]Electronic mail: matthew.mcgrath@helsinki.fi.

barriers),[39,40] though indirect molecular dynamics simulations (those which simulate a single, stable cluster in equilibrium with its surroundings) allow for an extension to points further from the spinodal.[38,41] As molecular dynamics is not used in this paper, we forgo an in-depth discussion of the topic and instead direct the reader to the excellent review of Kalikmanov *et al.*,[5] which is recent enough to include all but a few argon nucleation studies by molecular dynamics.[38,41–44]

A variety of Monte Carlo algorithms have been developed to study homogeneous vapor-liquid nucleation, starting with the work of Lee *et al.*,[45] who computed the Helmholtz free energy of clusters enclosed in a spherical volume. The canonical ensemble has been used in many Monte Carlo studies of argon since then, including work by Hale and Ward in 1982,[46] Hale again in 1996,[47] the n/v cluster work by Senger *et al.*,[25] the gauge cell/ghost field method of Neimark and Vishnyakov,[48,49] and the discrete summation method used by Lauri *et al.*[50] One can also consider the growth/decay algorithm of Vehkamäki and Ford[51,52] to be in the canonical ensemble, as it uses particle insertion and deletion moves (natural to the grand canonical ensemble) without ever accepting them to change the number of molecules in the simulation box. Other groups have found it more natural to work in the isobaric-isothermal ensemble, allowing one to specify the external pressure of the simulation, which can be a more convenient definition of the supersaturation.[53] The grand canonical ensemble allows one to add and remove molecules from the system, creating an inexpensive way to monitor the condensation and evaporation of a single cluster, and therefore it is also a natural choice for nucleation simulations;[54] the supersaturation can now be controlled through the value of the external chemical potential. Several groups have demonstrated the equivalence of their methods in multiple ensembles.[55,56]

While the properties of argon have made it very attractive for theoretical and simulation studies, difficulties have prevented its widespread exploration by experimental means. Initial studies in a supersonic nozzle (using helium as a carrier gas) were performed by Wu *et al.*[57] for temperatures lower than 45 K. A cryogenic shock tube was used in the studies of Zahoransky *et al.*,[58] who measured onset rates for temperatures between 48 and 85 K. The same group used a hypersonic shock tube several years later to give new estimates for the rates between 55 and 70 K.[59] Onset rates have also been measured for argon in a cryogenic pulse chamber at temperatures between 40 and 60 K.[60,61] A very recent study has used a cryogenic supersonic nozzle apparatus to explore temperatures from 34 to 53 K.[62] It should be noted that almost all of these experiments are at temperatures below the experimental triple point.

The aim of this work is to explore the effect of different intermolecular potentials in vapor-liquid nucleation. Previous studies of monatomic vapors have focused only on the Lennard-Jones potential (with a few forays into the nucleation of the Yukawa potential with classical density functional theory)[30,37,63–65] although some sensitivity studies have been done with water.[66–69] These studies found a significant effect of the interaction potential on nucleation properties, without an in-depth analysis to account for the difference in macroscopic properties predicted by the models. A very recent study by Parra and Graña[70] suggests that there should be no effect in classical density functional theory as long as the potential asymptotically decays as r^{-6} or faster. Classical nucleation theory has no dependence on the interaction between atoms; if two potentials produce the same macroscopic properties (e.g., vapor pressure, liquid density, and surface tension), CNT predicts they will show identical nucleation behavior. Given that vapor-liquid equilibrium is very sensitive to the intermolecular potential used,[71] one wonders if the implicit assumption is accurate. Molecular simulation and density functional theory are both capable of testing this assumption, as they both require explicit definition of the intermolecular potential; it is for this reason why both are used in this work. Classical nucleation theory, its extensions, and density functional theory have been explored in great depth elsewhere (see, for example, the reviews listed above). The following section, therefore, will highlight the major results of both classical nucleation theory and density functional theory. Section III enumerates the details of the Monte Carlo simulations, including the algorithms used, and Sec. IV presents the results of the theoretical calculations and molecular simulations along with a discussion. Section V summarizes the present work.

II. THEORETICAL BACKGROUND

A. Classical nucleation theory

Standard textbooks (such as Henderson)[72] and many reviews in the literature (see, for example, Oxtoby)[2] contain discussions of classical nucleation theory, with literature reviews often covering various extensions to the standard theory as well. The theory considers the formation of a spherical liquid droplet in a supersaturated vapor phase by expressing the free energy of formation of a cluster as being equal to the free energy penalty of creating a spherical interface minus the free energy benefit of converting metastable vapor to a stable bulk liquid phase. By invoking the capillarity approximation, one arrives at the free energy of formation of the critical nucleus (alternatively labeled ΔG^*, ΔW^*, or $\Delta\Omega$),

$$\Delta G^*_{\mathrm{CNT}} = \frac{16\pi\gamma^3}{3\rho_{\mathrm{l}}^2(k_{\mathrm{B}}T\ln S)^2}, \tag{1}$$

and the number of molecules present as

$$N^*_{\mathrm{CNT}} = \frac{32\pi\gamma^3}{3\rho_{\mathrm{l}}^2(k_{\mathrm{B}}T\ln S)^3}, \tag{2}$$

where γ is taken to be the surface tension of the planar liquid-vapor interface, ρ_{l} is the saturated liquid density, and S is the saturation ratio of the metastable vapor phase. In this work, the saturation ration is defined in terms of the chemical potential

$$S = \exp\left\{\frac{\mu_{ss} - \mu_s}{k_B T}\right\}, \tag{3}$$

where μ_{ss} and μ_s are the chemical potentials of the supersaturated and saturated phases. The nucleation rate is related to the formation free energy of the critical cluster by

$$J = J_o \exp\left\{\frac{-\Delta G^*}{k_B T}\right\}, \tag{4}$$

where the pre-exponential factor, J_o, is well-known.[5]

B. Density functional theory

The formalism of density functional theory has been covered in detail elsewhere (see, for example Zeng and Oxtoby,[31] or the excellent review by Laaksonen *et al.*[73]), and therefore only an overview of the main results will be presented here. The motivation behind the theory is to express the intrinsic free energy of a system as a functional of the density. Using a perturbative approach, the intrinsic free energy of a system described by any potential energy function that can be decomposed into a steeply repulsive part [the reference potential, $\phi^{(1)}(\mathbf{r})$] and a small attractive part [the perturbation, $\phi^{(2)}(\mathbf{r})$] is

$$F[\rho] \approx \int d\mathbf{r} f_h[\rho(\mathbf{r})] + \frac{1}{2}\int\int d\mathbf{r} d\mathbf{r}' \phi^{(2)}(|\mathbf{r} - \mathbf{r}'|)\rho(\mathbf{r})\rho(\mathbf{r}'), \tag{5}$$

where the first term is the Helmholtz free energy of the hard-sphere reference system, and both the random phase and local density approximations have been applied. One can obtain the grand potential of an inhomogeneous system by using the Helmholtz free energy

$$\Omega[\rho] = F[\rho] - \mu\int d\mathbf{r}\rho(\mathbf{r}). \tag{6}$$

The equilibrium density of the system is the one that minimizes this function. Taking the functional derivative of Eq. (6) with respect to the density profile, setting it equal to zero, and using Eq. (5) and a little algebra results in

$$\mu_h[\rho(\mathbf{r})] = \mu - \int d\mathbf{r}'\rho(\mathbf{r}')\phi^{(2)}(|\mathbf{r} - \mathbf{r}'|). \tag{7}$$

This equation can be solved by iteration to generate the equilibrium density profile for a liquid-vapor interface. That is, one guesses an initial density profile, $\rho(\mathbf{r})$. At each point of this profile and using a given equilibrium chemical potential, one can calculate the right-hand side of Eq. (7). Since μ_h is single-valued, it is inverted to give a new guess of the density at that point. One can also use Eq. (7) to find the size of the critical nucleus in vapor-liquid nucleation, though more care must be taken as the vapor droplet is a metastable system, and either evaporates or condenses in the limit of an infinite number of iterative steps. This procedure is described more below.

In order to perform the iterative procedure above, one needs to know the value of the chemical potential at equilibrium. It is well-known that the condition for phase coexistence is equality of the temperatures, pressures (in the case of a planar surface), and chemical potentials of each phase. In the case of a specified temperature, this gives two simultaneous equations: $\mu_l(T) = \mu_g(T)$ and $p_l(T) = p_g(T)$. In density functional theory, both of these quantities (the chemical potential and the pressure) can be written as functions of the homogeneous density. In the two phase region, a solution can be found such that $\rho_g \neq \rho_l$; however, the success in finding these values depends on the quality of the initial guess of densities.

One can quickly derive expressions for both the free energy, pressure and chemical potential of the homogeneous systems from Eqs. (5) and (7) above: $f(\rho) = f_h(\rho) - \frac{1}{2}\alpha\rho^2$, where $\alpha = -\int d\mathbf{r}' \phi^{(2)}(\mathbf{r}')$ (see, for example, Zeng and Oxtoby[31] for the other two relations). The free energy, pressure, and chemical potential of hard-spheres were computed in this work by the Carnahan–Starling equations.[74]

Up until now, no mention has been made of the intermolecular potential, save that it be separable into a steeply repulsive part and a small, perturbative attractive part. We adopt the Weeks, Chandler, and Anderson (WCA) approach.[75] The attractive part of the potential can then be written as

$$\phi_2^{WCA}(r) = \begin{cases} -\epsilon, & r < r_{min} \\ \phi(r), & r \geq r_{min}, \end{cases} \tag{8}$$

where r_{min} and ϵ are the location of the deepest part of the potential well and its value, respectively.

In order to calculate the chemical potential, pressure, and free energy of the system, one still needs to select a diameter for the reference system of hard-spheres. It is common to use the temperature-dependent hard-sphere diameter of Lu–Evans–Telo da Gama,[76] but as the Monte Carlo calculations in this work require the calculation of precise values of the saturated liquid and vapor densities for every potential (along with the surface tension) it seemed more prudent to adapt a semiempirical approach for the DFT nucleation calculations, similar to the work of Nyquist *et al.*[37] and Laasonen *et al.*[39] Instead of fitting all the potential parameters to the simulation data, we decided to only adjust the hard-sphere diameter, as searching the full parameter space of the more complex potentials above is not feasible (a single simulation point can take hours). The value used for the nucleation simulations was the value which minimized the unsigned error between the Monte Carlo simulation results for the saturated densities and surface tension and the quantities calculated from DFT. The error in each of the three properties was less than 10% between the best-fit values and the simulation values, with the best fitting occurring with the Barker–Fisher–Watts potential; there, errors of only a few percent were found. The starting value was the Lu–Evans–Telo da Gama diameter and the best-fit was found within 2% of this value.

As mentioned above, Eq. (7) can also be solved to give the critical cluster size for homogeneous vapor-liquid nucleation. Here, however, μ is the chemical potential of the supersaturated vapor phase and the interface is not stable. If the initial cluster radius is too small, the droplet evaporates; if it

is too large, the droplet condenses. If the initial cluster size is close to that of the critical cluster, however, it takes many iterations for it to disappear. A plot of the number of excess molecules in the cluster ($N_{ex}=\int d\mathbf{r}[\rho(\mathbf{r})-\rho_{ss}]$, where ρ_{ss} is the supersaturated vapor density) shows a plateau. A reasonable definition of "convergence" in this case is 30 iteration steps with a change in cluster size of less than 0.1 molecules. The activation barrier height is given as the difference in the grand potential of the supersaturated and saturated systems,

$$\Delta\Omega_{DFT}=\Omega_{ss}-\Omega[\rho_v]=\Omega_{ss}+p[\rho_v]. \tag{9}$$

One typically computes the nucleation rate from this value by substituting it in the expression for the classical nucleation rate above [Eq. (4)], maintaining the same value of the pre-exponential factor.

The lack of random variables makes it more difficult to estimate the uncertainty in the nucleation results for density functional theory. Instead, the effect of changing the number of grid points used to represent the density and the maximum number of iterations allowed in the nucleation calculations was examined. It was found that doubling each of these values for the Lennard-Jones system at 70 K changed $\Delta\Omega^*$ and n^* by less than 0.001%, which is less than the uncertainties for either of the other methods; therefore, the uncertainties for the DFT calculations are omitted for clarity.

III. SIMULATION DETAILS

All of the theory presented until this point is completely general. No details of the interaction potentials have been given, save that (in the case of DFT) they must be pair potentials. We now introduce the specific intermolecular potentials to be used in the following calculations. It should be noted that details of the procedure for computing vapor-liquid nucleation with the grand canonical version of the aggregation-volume-bias algorithm with umbrella sampling (AVUS) have been reported several times by Chen *et al.*,[56,77] including the use of histogram-reweighting.[69,78]

A. Intermolecular potentials

The Lennard-Jones potential is an effective potential that accurately and quickly reproduces a wide range of macroscopic properties. Its form is given by

$$U_{LJ}(r)=4\epsilon\left[\left(\frac{\sigma}{r}\right)^{12}-\left(\frac{\sigma}{r}\right)^{6}\right]. \tag{10}$$

Potoff and Panagiotopoulos[79] accurately determined the critical properties for the monatomic Lennard-Jones fluid in reduced units: $T_c^*=1.3120=k_BT_c/\epsilon$, $\rho_c^*=0.316=N_c\sigma^3/V_c$, and $p_c^*=0.1279=p\sigma^3/\epsilon$. By using the experimental values of the critical properties of argon, we can use these formulas to compute the values of ϵ and σ for each element. These results are given in Table I.

The form of the Lennard-Jones potential is not perfect, however. The repulsive r^{-12} part of the potential has been shown to rise too steeply compared to quantum mechanical data at small separations, while a modified Buckingham exponential-six potential better reproduces the experimental data.[81] The form of the modified Buckingham exponential-six potential is given by Mason and Rice,[82]

$$U_{BUCK}(r)=\frac{\epsilon}{1-\frac{6}{\alpha}}\left[\frac{6}{\alpha}\exp\left[\alpha\left(1-\frac{r}{r_m}\right)\right]-\left(\frac{r_m}{r}\right)^6\right], \tag{11}$$

who have also determined values of α, ϵ, and r_m for argon, krypton, and xenon. These parameters are given in Table II.

Vapor-liquid equilibrium has long been known to be very sensitive to the interaction potential used; in particular, the simple act of truncating and shifting a Lennard-Jones potential at 2.5σ has been shown to have significant effects.[71] This, combined with the importance of three-body effects in the simulation of noble gases,[83,84] led the authors to initially eschew the use of any strictly two-body interaction potentials in this work (the two potentials listed above are "effective" pair potentials, which implicitly include many-body effects in their fitting to experimental data). However, it was decided that the use of the Barker–Fisher–Watts (BFW) potential for argon[85] could serve as an interesting test case to see if the sensitivity to potential parameters observed in vapor-liquid equilibrium is also observed in vapor-liquid nucleation. The pairwise BFW potential energy is given by

$$U_{BFW}(r)=\epsilon\left[\sum_{i=0}^{5}A_i\left(\frac{r}{r_m}-1\right)^i\times\exp\left[\alpha\left(1-\frac{r}{r_m}\right)\right]-\sum_{j=0}^{2}\frac{C_{2j+6}}{\delta+\left(\frac{r}{r_m}\right)^{2j+6}}\right], \tag{12}$$

and the parameters used for argon are given in Table III.

In addition, recent studies have produced effective potentials from *ab initio* dimer data for both argon[86] and krypton[87] that show good agreement with experimental critical properties. This was done by computing an "effective" diameter (ED) for the element over a large range of densities and temperatures, and then fitting the results to an empirical function of the form[86]

TABLE I. The experimental critical properties of argon (Ref. 80), along with the values of the Lennard-Jones parameters calculated using the reduced critical values of T_c^* and ρ_c^* of Potoff and Panagiotopoulos (Ref. 79).

	T_c (K)	ρ_c (mol/l)	p_c (bar)	ϵ/k_B (K)	σ (Å)
Ar	150.86	13.41	48.9805	114.98	3.40

TABLE II. The parameters of the exponential-six potential for argon (Ref. 82).

	α	r_m (Å)	ϵ/k_B (K)
Ar	14.0	3.866	123.2

TABLE III. The Barker–Fisher–Watts parameters for argon (Ref. 85). The functional form is given in Eq. (12).

ϵ/k_B (K)	142.095
σ (Å)	3.7612
A_0	0.277 83
A_1	−4.504 31
A_2	−8.331 215
A_3	−25.2696
A_4	−102.0195
A_5	−113.25
C_6	1.107 27
C_8	0.169 713 25
C_{10}	0.013 611
α	12.5
δ	0.01

$$U_{\mathrm{ED}}(R) = A\ \exp\{-\alpha R + \beta R^2\} + \sum_{n=3}^{6} \frac{C_{2n}}{R^{2n}}, \tag{13}$$

where $R=r/a_o$, r is the separation distance between two atoms, and a_o is the Bohr radius. For consistency with the other potentials, we will use the form

$$U_{\mathrm{ED}}(r) = A\ \exp\{-\alpha' r + \beta' r^2\} + \sum_{n=3}^{6} \frac{C'_{2n}}{r^{2n}}, \tag{14}$$

where the separation distance is given in angstroms and the values of the Bohr radius have been folded into the coefficients, distinguished with a " ′." The parameters used for argon are given in Table IV. A comparison of all the potentials for argon is given in Fig. 1. It is clear that all of the effective potentials give a well depth and effective radius that are similar, while the pure pair potential (BFW) is more strongly attractive.

It must be noted here that all potentials used in this work were truncated and shifted at a value of $5\times\sigma_{\mathrm{LJ}}$ (17.0 Å) in order to facilitate future comparisons with the results from molecular dynamics simulations. This means that no long-range corrections were used for the energy. Additionally, as a result of this rather long cutoff (which is the minimum suggested by Mecke *et al.*[88] for calculation of the surface tension of Lennard-Jonesium), corrections to the pressure and surface tensions resulting from the discontinuity in the force at the cutoff distance were not explicitly evaluated. However, using an approach suggested by Smit[71] the pressure correction is found to be less than 0.1%, i.e., smaller than the statistical uncertainties of the current simulations.

TABLE IV. The parameters of potentials fit to the effective diameters of argon (Ref. 86) as computed from *ab initio* data. The functional form is given by Eq. (14).

	Ar
A (K)	$5.582\ 991\ 3\times10^7$
α' (Å^{-1})	3.059 523 3
β' (Å^{-2})	−0.088 107 455
C'_6 (K Å^6)	$-4.610\ 072\ 7\times10^5$
C'_8 (K Å^8)	$-1.850\ 535\ 8\times10^6$
C'_{10} (K Å^{10})	$-6.096\ 920\ 1\times10^7$
C'_{12} (K Å^{12})	$1.863\ 958\ 4\times10^8$

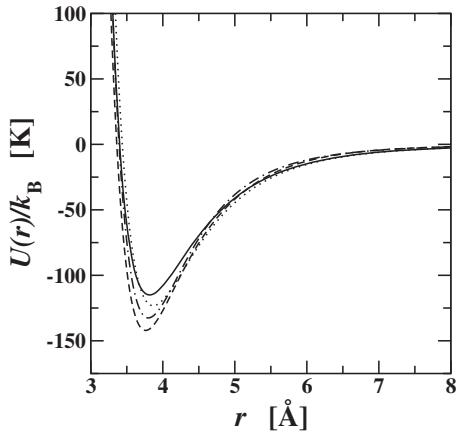

FIG. 1. Graphs of the intermolecular interaction potentials for argon used in this work. The Lennard-Jones, exponential-six, effective diameter, and Barker–Fisher–Watts potentials are given by solid, dotted, dashed-dotted, and dashed lines, respectively.

The temperatures explored in this work ($T=70$ and 90 K, or $T^*=0.609$ and 0.783 for the Lennard-Jones potential) were chosen to be slightly above and below the experimental triple point. Higher temperatures result in barrierless vapor-liquid nucleation for all except minimal supersaturations, while at lower temperatures the computation of the saturated vapor properties is more difficult and the liquid-solid transition occurs.[89] Only molecular translations were performed to thermally equilibrate the system and the maximum displacements were adjusted to give an acceptance rate of 50%.

B. Surface tension

In order to compute the surface tension, simulations were performed in the canonical (*NVT*) ensemble. A system of 1200 molecules was first equilibrated using the Lennard-Jones potential at the coexistence density for each temperature. Following 10^5 cycles of equilibration, the box length in the z-direction was doubled to produce the interface. Another 10^5 cycles of equilibration were run for all four potentials beginning from this configuration at each temperature. The value of the surface tension was then computed over 10^6 cycles by Salmons and Mareschal,[90]

$$\gamma = \frac{1}{2A}\langle 2V_{zz} - V_{xx} - V_{yy}\rangle = \frac{1}{2A}\left\langle \sum_{i<j}\left(r_{ij} - \frac{3z_{ij}^2}{r_{ij}}\right)u'(r_{ij})\right\rangle, \tag{15}$$

where the angular brackets denote an ensemble average, A is the total area of the interface ($A=2L_xL_y$ in this case), V_{xx}, V_{yy}, and V_{zz} are the directional components of the virial, r_{ij} and z_{ij} are the distance and the z component of the distance between molecules i and j, and $u'(r_{ij})$ is the first derivative of the energy with respect to the distance. The simulation was divided into five blocks of 2×10^5 cycles to estimate the error bars, which are computed as standard errors of the mean.

TABLE V. Experimental and calculated saturated properties of argon. LJ, BUCK, BFW, ED, and EXP refer to the Lennard-Jones, modified Buckingham exponential-six, Barker–Fisher–Watts, effective diameter potentials, and the experimental results, respectively. Values in parenthesis are the uncertainty in the last digit. The saturated chemical potential is computed from isobaric-isothermal simulations, while the other properties are calculated from simulations in the Gibbs ensemble. As 70 K is below the experimental triple point, experimental values are not available for the metastable liquid.

	T (K)	ρ_v (g/cm^3)	ρ_l (g/cm^3)	γ (mN/m)	p_v (kPa)	μ/k_B (K)
LJ	70.0	0.001 05(2)	1.4771(2)	16.8(2)	15.2(1)	−1007.47(1)
ED	70.0	0.000 81(1)	1.5031(4)	16.5(2)	11.7(2)	−1025.71(1)
BUCK	70.0	0.000 676(7)	1.4410(3)	17.4(2)	9.8(1)	−1038.04(1)
BFW	70.0	0.000 34(1)	1.5714(3)	20.2(2)	4.9(1)	−1086.40(1)
EXP	70.0	⋯	⋯	⋯	⋯	⋯
LJ	90.0	0.009 99(3)	1.3501(2)	11.6(1)	178.3(5)	−1133.73(1)
ED	90.0	0.0088(1)	1.3842(3)	11.6(1)	158(1)	−1144.32(2)
BUCK	90.0	0.007 26(3)	1.3280(1)	12.2(1)	130.8(6)	−1160.81(2)
BFW	90.0	0.004 63(4)	1.4614(3)	14.6(1)	84.4(7)	−1199.19(1)
EXP	90.0	0.007 44	1.3786	11.9	133.5	⋯

C. Chemical potential

Initially, the Gibbs ensemble Monte Carlo technique (GEMC)[91–93] was used to accurately compute the value of the saturated vapor phase chemical potential. The move probabilities were adjusted to give approximately one accepted molecular swap and one accepted volume displacement every ten cycles, except at lower temperatures where the swap move acceptance is significantly lower. Here, the swap move trial percentage was never allowed to exceed 30%. Approximately 5×10^4 cycles of equilibration were run, followed by production runs of 10^6 cycles for which the saturated liquid and vapor properties were computed. The long production periods were necessary because, according to classical nucleation theory, critical cluster sizes depend on the cube of the supersaturation [see Eq. (2)]; therefore, small uncertainties in the chemical potential [which is used to compute the supersaturation by Eq. (3)] can cause large uncertainties in the simulation conditions. The simulations were divided into five blocks of 2×10^5 cycles to calculate the standard error of the mean for each property.

After following the above GEMC procedure, it was noticed that the uncertainties in the saturated chemical potentials were still approaching the magnitude of the chemical potential difference for the supersaturations used in this work. Therefore, an alternative procedure was used. Monte Carlo simulations were run in the isobaric-isothermal (NpT) ensemble using 120 molecules and an external pressure equal to the vapor pressure obtained from the GEMC simulations above. These simulations were run for 10^7 cycles and the chemical potential was calculated by the Widom particle insertion method,[94]

$$\mu = -k_B T \ln\left(\Lambda^{-3}\left\langle \frac{V}{N+1}\exp\left[-\frac{U}{k_B T}\right]\right\rangle\right). \tag{16}$$

Here, V is the volume of the simulation box, N is the number of molecules of this type in the box, U is the energy of the inserted molecule, and the angular brackets represent the ensemble average. The simulations were divided into ten equal blocks in order to calculate the standard error of the mean, which was reduced by an order of magnitude from the GEMC simulations. As the systems contained more than one hundred molecules, no system-size correction was applied to the chemical potential.[95,96]

D. Aggregation-volume umbrella sampling Monte Carlo with histogram-reweighting

For the nucleation simulations, an aggregation-volume-bias grand canonical algorithm with umbrella sampling and histogram-reweighting (AVUS-HR) was used, which simulates an isolated cluster that increases and decreases in size via the grand canonical particle swap moves. The details of the algorithm are given in depth by Chen *et al.*[56,69] The aggregation-volume-bias Monte Carlo (AVBMC) algorithm[97,98] defines "inner" and "outer" radii for the swap moves to a target molecule; since the Stillinger cluster criterion[99] was used here, it was natural to use the same distance for the "outer" AVB radius. The cutoff distance was chosen to be $1.5\sigma_{LJ}$ (5.1 Å) for all potential models. The use of configurational bias Monte Carlo[100] increases the acceptance rates for the AVBMC swap moves, thus enhancing efficiency. The histogram-reweighting technique[101] has the advantage of being able to extract information about neighboring state points from a single simulation and therefore only two explicit simulations were run for each model/parameter set (see Table V). The histogram-reweighting method applied to AVUS simulations is discussed by Chen *et al.*[69] The biasing potential for the umbrella sampling technique[102] was adjusted at regular intervals by a self-adapting scheme in order to give a function equal to the negative of the true free energy barrier, in accordance with the method described by Chen *et al.*[56] This involved assembling the curve in piecewise intervals before running a long simulation of 10^7 cycles, the histograms values from which were used to smooth the whole curve. An effort to calculate the uncertainty in the barrier height and critical cluster from this approach was made by calculating the standard errors of

TABLE VI. Calculated values of the nucleation energy barrier for argon. The subscripts MC, CNT, and DFT refer to the values calculated from Monte Carlo simulations, classical nucleation theory, and density functional theory, respectively. Values in parenthesis are the uncertainty in the last digit. As explained in the text, the estimated uncertainty for the DFT calculations is less than 0.001%.

	T (K)	S	$\Delta W^*_{MC}/k_BT$	n^*_{MC}	$\Delta W^*_{CNT}/k_BT$	n^*_{CNT}	$\Delta W^*_{DFT}/k_BT$	n^*_{DFT}
LJ	70.0	5.0	55.5(1)	89(1)	69(2)	85(3)	57.0	90.3
ED	70.0	5.0	53.9(1)	85(1)	63(2)	78(3)	57.5	87.1
BUCK	70.0	5.0	68.4(1)	104(1)	80(3)	99(3)	71.9	107.4
BFW	70.0	5.0	87.7(1)	127(2)	105(3)	130(4)	108.5	150.8
LJ	90.0	2.5	26.5(1)	90(1)	39(2)	85(4)	24.2	80.6
ED	90.0	2.5	25.5(1)	82(1)	37(1)	81(2)	24.3	75.5
BUCK	90.0	2.5	37.4(1)	111(2)	47(1)	103(3)	39.1	111.3
BFW	90.0	2.5	54.0(1)	143(1)	67(1)	146(3)	63.2	160.7

the mean across four independent runs of 2×10^5 cycles; these errors are low enough that no effort was made to calculate independent runs of the full 10^7 cycles.

As no experimental nucleation rates exist for argon at elevated temperatures (Iland *et al.*[61] give results for 42–58 K), the supersaturation ratios traditionally chosen in theoretical studies are somewhat arbitrary. Therefore, the conditions in this paper were chosen such that the explicit AVUS-HR simulations for the Lennard-Jones potential gave critical cluster sizes of around 100 atoms. This resulted in supersaturation ratios of 5.0 and 2.5 for 70 and 90 K, respectively, which lie in the region commonly explored in theoretical studies.[5]

IV. RESULTS AND DISCUSSIONS

In order to precisely determine the nucleation conditions (in particular, the supersaturation), very precise values for the chemical potential must be obtained. The results of the GEMC and NpT simulations are shown in Table V. From this table, it can be seen that the LJ and the ED potentials reproduce the experimental densities most closely, while the BUCK potential gives an accurate estimate of the vapor pressure and the BFW potential giving the most significant deviation. As mentioned above, this result is unsurprising given that both the Lennard-Jones potential and the effective diameters potential are effective potentials and parametrized to reproduce experimental data, while the Barker–Fisher–Watts potential was developed as a pure two-body potential and consequently does not contain (even in an averaged sense) the three-body effects which are know to be important in the studies of noble gases.[83]

The results of the Monte Carlo AVUS, classical density functional theory, and classical nucleation theory calculations are shown in Table VI. From this table, it can be seen quite clearly that the different intermolecular potentials result in different nucleation behavior at the same absolute temperature and saturation ratio. Another interesting trend noticed in this table is that the semiempirical DFT calculations (in which the hard-sphere diameter is varied to reproduce the macroscopic surface tension and saturation properties found in Monte Carlo simulations) give better agreement with the MC results than classical nucleation theory (in which the macroscopic properties used are those found from Monte Carlo simulations), insofar as the formation free energies are concerned for three of the potentials studied. This agrees with previous observations.[38] The disagreement between the nucleation results obtained by DFT and MC for the BFW potential is explored more below.

One of the consequences of comparing different intermolecular potentials is the possibility that the potentials predict different macroscopic properties. As can be seen in Table V, this is certainly true in this work. As classical nucleation theory predicts that the nucleation behavior depends on the macroscopic properties of the system, it stands to reason that potentials predicting different properties could predict different nucleation behavior, as well. In order to remove this influence on these studies, Figs. 2 and 3 show the size and

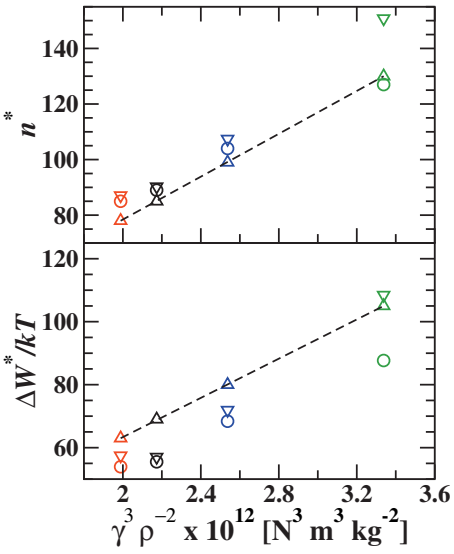

FIG. 2. The number of molecules in (top) and the free energy of formation of (bottom) the critical nucleus of argon at $T=70$ K and $S=5$ for all methods used in this work, shown as a function of the cube of the computed surface tension divided by the square of the saturated liquid density. Circles, triangles-up, and triangles-down represent results from the Monte Carlo simulations, classical nucleation theory, and density functional theory, respectively. Black, red, blue, and green indicate results for the Lennard-Jones, effective diameter, Buckingham exponential-six, and Barker–Fisher–Watts potentials, respectively. The dashed line connects the results for classical nucleation theory as a guide to the eyes.

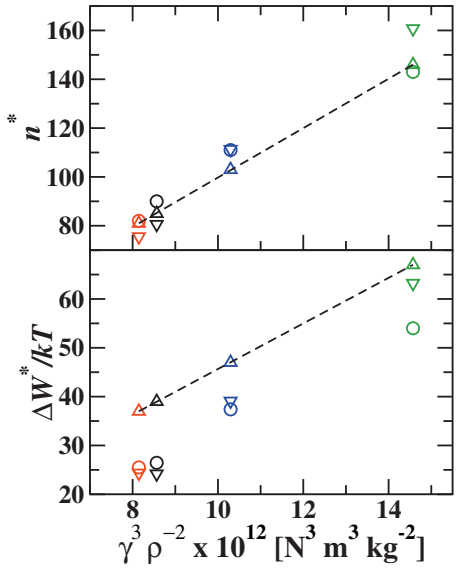

FIG. 3. The number of molecules in (top) and the free energy of formation of (bottom) the critical nucleus of argon at $T=90$ K and $S=2.5$ for all methods used in this work, shown as a function of the cube of the computed surface tension divided by the square of the saturated liquid density. The legend is the same as in Fig. 2.

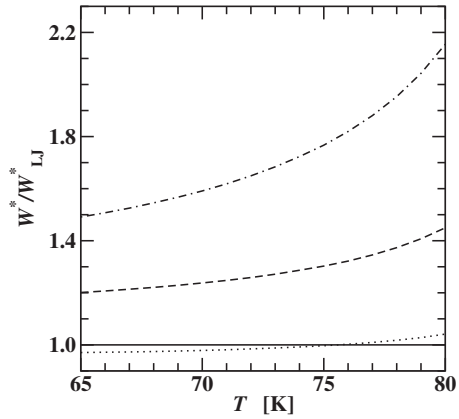

FIG. 4. The ratio of the free energy of formation of the critical nucleus for each of the four potentials explored in this work divided by the same quantity for the Lennard-Jones potential as a function of temperature. The solid, dotted, dashed, and dashed-dotted lines depict the Lennard-Jones, effective diameter, Buckingham-6, and Barker–Fisher–Watts potentials, respectively.

formation free energy of the critical cluster as a function of the saturated liquid density and the surface tension ($\gamma^3\rho^{-2}$) for both 70 and 90 K. This particular quantity was chosen so that the results from classical nucleation theory would give a straight line [see Eqs. (1) and (2)], as indeed they do. It is important to note here that neither axis on these plots is independent (i.e., the potential used and temperature dictate both the macroscopic properties as well as the nucleation behavior). As can be seen in Figs. 2 and 3, properties of the critical clusters in both the MC and DFT calculations do not have the same dependence on the critical properties that CNT predicts, although the free energies of formation for the MC simulations give a roughly straight line with a slope similar to that of CNT. Given that the estimated errors for the simulations are smaller than the symbols on the graph, this difference is thought to be significant; however, given the uncertainty also in the x-axis values, much longer simulations are required to be sure.

One feature of both Figs. 2 and 3 is the relative position of the free energy of formation for DFT compared to MC and CNT for the BFW potential. A recent study[70] suggests that if two potentials have the same asymptotic decay (and it is greater than or equal to r^{-6}), the specific form of the potential should have little impact on the nucleation behavior in density functional theory. All of the potentials used in this study have an asymptotic decay of r^{-6}, and yet the Barker–Fisher–Watts potential seems to exhibit different behavior than the other three potentials. Given that modification of the hard-sphere diameter led to a smaller error in the DFT-calculated saturated densities and liquid-vapor surface tension (compared to the MC results) for the BFW potential than the other three potentials, the source of this discrepancy is unclear.

The use of the histogram-reweighting technique[69] allows one to predict the free energy barriers at additional simulation conditions (temperature and supersaturation) where one has not explicitly used the AVUS technique. Histogram-reweighting is exact when one knows the precise value of the chemical potential. For an ideal gas, this can be quickly related to the number density,[78] which in turn is linked to the vapor pressure by using the ideal gas equation-of-state. This means that if one knows the vapor pressure of an ideal gas phase, one can quickly compute the free energy barrier from a simulation at a neighboring temperature. It was noticed here that the vapor phase at 90 K is nonideal enough that this conversion cannot be used without introducing error. As this study is concerned only with exploring the differences between the intermolecular potentials used, it was decided that the histogram-reweighting technique would only be used for temperatures from 65 to 80 K, where the vapor phase of all potentials is still fairly ideal; this would be sufficient to examine any differences. In order to determine the saturated vapor pressure across this range, additional GEMC simulations following the procedure outlined in Sec. III C were performed at 80 K for all four potentials, and the resulting vapor pressure was used to determine a linear least-squares line from the Clausius–Clapeyron equation (the third temperature was added to confirm the linear relationship between $\ln p_{sat}$ and $1/T$). The data resulting from the application of the histogram-reweighting technique are plotted in Fig. 4, showing the formation free energy of the critical nucleus for various temperatures at a saturation ratio of 5.0. This quantity is normalized by the Lennard-Jones free energy under the same conditions, in order to better illustrate any differences. It can be seen from this plot that the different potentials do not exhibit the same temperature dependence, which lends further credence to the idea that the interaction potentials themselves are influencing the behavior of the system.

An obvious question that arises during the previous series of analyses is: are the differences seen a result of the difference in macroscopic properties of the system? While there is no clear way to address this, the law of corresponding states suggests that if one compares results at the same reduced temperature ($T^*=T/T_c$), one might see similar behavior. In order to test this, one needs to know the critical

TABLE VII. Critical temperatures, the free energy of formation of the critical cluster (for all three methods), and the slope of the free energy of formation as a function of temperature for both a constant absolute temperature and a constant reduced temperature ($T^*=T/T_c$) for all four potentials used in this work. The numbers in parentheses are the calculated uncertainty in the final digit. T and T^* refer to values at constant absolute temperature ($T=70$ K) and reduced temperature ($T^*=0.480$).

	T_c (K)	$\Delta W^*_{MC}/k_BT$		$\frac{\Delta\Delta W^*_{MC}/k_BT}{\Delta T}$		$\Delta W^*_{CNT}/k_BT$		$\Delta W^*_{DFT}/k_BT$	
		$[T]$	$[T^*]$	$[T]$	$[T^*]$	$[T]$	$[T^*]$	$[T]$	$[T^*]$
LJ	145.9(3)	55.5	54.3	−5.34	−5.34	69(2)	69(2)	57.0	57.0
ED	147.6(3)	53.9	47.8	−5.14	−4.51	63(2)	64(2)	57.5	52.5
BUCK	151.3(3)	68.4	47.5	−6.12	−4.74	80(3)	65(1)	71.9	54.5
BFW	160.0(4)	87.7	48.2	−7.11	−4.61	105(3)	60(1)	108.5	58.2

properties of all the models used in this work. While these data are available from Potoff and Panagiotopoulos[79] (compared to the experimental data for argon),[80] Errington and Panagiotopoulos,[103] Nasrabad and Laghaei,[86] and Tsona,[104] the potentials used there do not strictly follow the truncation/shifting procedure in this work. As this is known to have a significant effect on the critical properties of Lennard-Jonesium,[71] simulations were performed following the GEMC procedure outlined above. In order to conserve computer time, the production period was limited to 2×10^5 cycles and the production was divided into five equal-length runs to estimate the statistical uncertainty. The critical temperatures in Table VII were computed by fitting saturated liquid and vapor densities near the critical temperature to the traditional scaling relationships, using a universal Ising exponent $\beta=0.325$ and no finite-size scaling.[105]

With the predicted critical temperatures for each model, one can now examine the nucleation free energy barrier as well as its temperature dependence. This information is given in Table VII. The difference between the Monte Carlo results for Lennard-Jones at $T=70$ K and $T^*=0.480$ is due to the fact that this latter quantity is taken from the histogram-reweighting procedure, which includes information from multiple state points. This table demonstrates that when one considers the difference in critical temperatures predicted by the potentials, the free energy of formation of the critical cluster (as well as its temperature dependence) becomes much more independent of the potential used; however, some small differences remain. It is interesting to note that in this table, the Lennard-Jones potential produces results that differ the most significantly from the other three potentials, while in Figs. 2 and 3 it was the Barker–Fisher–Watts potential which disagreed with the other potentials. Again, the reason for this discrepancy is unclear, but the fact that it occurs during two different methods of analysis for two different potentials suggests that there is no simple scaling factor to transform the results for one potential into another.

It is instructive to examine the structural properties of the clusters as well as the energetics. Figure 5 is a plot of the logarithm of the number of molecules in a cluster as a function of the logarithm of the radius of gyration at the lower temperature explored in this work (the figure for the higher temperature is similar). Chen *et al.*[56] performed a similar analysis for Lennard-Jones clusters at various temperatures and saturation ratios. Several of their observations are also pertinent here, including that all of the curves show a pronounced S-shape. This indicates that the fractal dimension of the cluster does not smoothly go from 2 (at the smaller clusters) to 3 (at the larger), but instead makes a very rapid change at intermediate cluster sizes. This effect is the most pronounced for LJ and the least for BFW, which agrees with another of the observations made by Chen *et al.*;[56] this shape transition shifts toward larger cluster sizes as the temperature increases. Although this result may not be obvious, it appears when one considers the reduced temperature of the simulation instead of the absolute temperature. As BFW has the largest critical temperature, $T=70$ K represents the smallest reduced temperature (out of the four potentials) and the location of the transition cluster in Fig. 5 is correspondingly the lowest as well. However, it must be noted that this trend does not hold true for every potential; the three effective potentials used in this work are not similarly ordered (the positions of BUCK and ED are reversed, relative to their critical temperature), which reiterates the observation made above that, even accounting for differences in macroscopic properties, the intermolecular potential appears to influence homogeneous vapor-liquid nucleation.

V. CONCLUSION

Monte Carlo simulations and classical density functional theory calculations exploring the homogeneous vapor-liquid

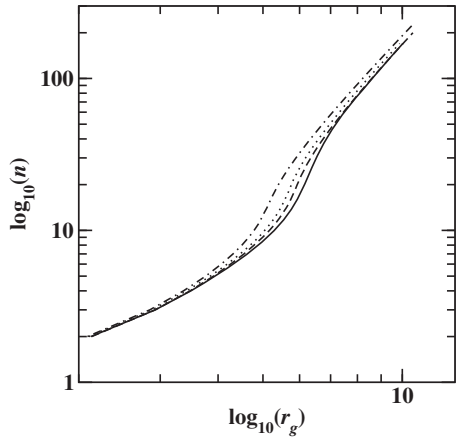

FIG. 5. The number of molecules in a given cluster as a function of the radius of gyration for $T=70$ K. The legend is the same as in Fig. 4.

nucleation behavior of argon were performed for four different descriptions of the intermolecular energy. These results were compared to the predictions by classical nucleation theory (which depends only on the macroscopic properties predicted by the models) in order to determine if the nucleation behavior of argon is dependent on the intermolecular potential used. It was found that the different potentials produced significantly different results at the same absolute temperature, which is in agreement with previous sensitivity studies performed on water. A more in-depth analysis revealed that neither the Monte Carlo simulations nor the calculations with semiempirical density functional theory follow the same dependence on macroscopic properties as classical nucleation theory (although the results for the Monte Carlo simulations are similar, at least for the formation free energy of the critical cluster). Use of the histogram-reweighting technique to compute the temperature dependence of the critical cluster free energy around the lower (more ideal) temperature showed significant differences as well. Attempts to compensate for the difference in critical temperatures predicted by the models (by comparing data at the same reduced temperature) reduced the differences for the temperature dependence as well as the formation free energies, but it did not eliminate them. This observation agrees with a recent study performed with only classical density functional theory (using different potentials than those employed in this work)[70] and suggests that the failing of classical nucleation theory is related to (among other things) an improper consideration of the molecular interactions.

ACKNOWLEDGMENTS

M.J.M. gratefully acknowledges support from a National Science Foundation International Research grant (Grant No. OISE-0853294). J.I.S. would like to acknowledge support from NSF Grant No. CBET-0756641. B.C. gratefully acknowledges NSF Grant No. CHE/MCB-0448918. I.N. and H.V. gratefully acknowledge funding from the Academy of Finland (LASTU Research Programme). The authors also gratefully acknowledge the donation of computers to the Department of Chemistry, Faculty of Science, University of Dschang by the Peace Corps-Cameroon on behalf of Montgomery County, Maryland, USA. Part of the computing resources was provided by the Minnesota Supercomputing Institute and CSC, Helsinki.

[1] J. H. Seinfeld and S. N. Pandis, *Atmospheric Chemistry and Physics: From Air Pollution to Climate Change* (Wiley, New York, 1998).
[2] D. W. Oxtoby, J. Phys.: Condens. Matter **4**, 7627 (1992).
[3] J. D. Gunton, J. Stat. Phys. **95**, 903 (1999).
[4] B. Senger, P. Schaaf, D. S. Corti, R. Bowles, J.-C. Voegel, and H. Reiss, J. Chem. Phys. **110**, 6421 (1999).
[5] V. I. Kalikmanov, J. Wölk, and T. Kraska, J. Chem. Phys. **128**, 124506 (2008).
[6] R. Becker and W. Döring, Ann. Phys. **416**, 719 (1935).
[7] H. Reiss, J. Chem. Phys. **18**, 840 (1950).
[8] D. Kashchiev, J. Chem. Phys. **76**, 5098 (1982).
[9] H. Reiss, A. Tabazadeh, and J. Talbot, J. Chem. Phys. **92**, 1266 (1990).
[10] D. W. Oxtoby and D. Kashchiev, J. Chem. Phys. **100**, 7665 (1994).
[11] R. McGraw and A. Laaksonen, Phys. Rev. Lett. **76**, 2754 (1996).
[12] I. J. Ford, Phys. Rev. E **56**, 5615 (1997).
[13] V. Talanquer, J. Chem. Phys. **106**, 9957 (1997).
[14] K. Koga and X. C. Zeng, J. Chem. Phys. **110**, 3466 (1999).
[15] M. P. Moody and P. Attard, J. Chem. Phys. **117**, 6705 (2002).
[16] S. V. Vosel, A. A. Onischuk, and P. A. Purtov, J. Chem. Phys. **131**, 204508 (2009).
[17] A. Dillmann and G. E. A. Meier, J. Chem. Phys. **94**, 3872 (1991).
[18] C. F. Delale and G. E. A. Meier, J. Chem. Phys. **98**, 9850 (1993).
[19] V. I. Kalikmanov and M. E. H. van Dongen, J. Chem. Phys. **103**, 4250 (1995).
[20] I. J. Ford, A. Laaksonen, and M. Kulmala, J. Chem. Phys. **99**, 764 (1993).
[21] G. K. Schenter, S. M. Kathmann, and B. C. Garrett, Phys. Rev. Lett. **82**, 3484 (1999).
[22] K. J. Oh, X. C. Xeng, and H. Reiss, J. Chem. Phys. **107**, 1242 (1997).
[23] P. Schaaf, B. Senger, and H. Reiss, J. Phys. Chem. B **101**, 8740 (1997).
[24] P. Schaaf, B. Senger, J.-C. Voegel, and H. Reiss, Phys. Rev. E **60**, 771 (1999).
[25] B. Senger, P. Schaaf, D. S. Corti, R. Bowles, D. Pointu, J.-C. Voegel, and H. Reiss, J. Chem. Phys. **110**, 6438 (1999).
[26] D. Reguera, R. K. Bowles, Y. Djikaev, and H. Reiss, J. Chem. Phys. **118**, 340 (2003).
[27] V. I. Kalikmanov, J. Chem. Phys. **124**, 124505 (2006).
[28] D. Reguera and H. Reiss, Phys. Rev. Lett. **93**, 165701 (2004).
[29] R. Zandi, D. Reguera, and H. Reiss, J. Phys. Chem. B **110**, 22251 (2006).
[30] D. W. Oxtoby and R. Evans, J. Chem. Phys. **89**, 7521 (1988).
[31] X. C. Zeng and D. W. Oxtoby, J. Chem. Phys. **94**, 4472 (1991).
[32] V. Talanquer and D. W. Oxtoby, J. Chem. Phys. **100**, 5190 (1994).
[33] V. Talanquer and D. W. Oxtoby, J. Phys. Chem. **99**, 2865 (1995).
[34] J. Barrett, J. Chem. Phys. **107**, 7989 (1997).
[35] D. Reguera and H. Reiss, J. Chem. Phys. **120**, 2558 (2004).
[36] L. Gránásy, Z. Jurek, and D. W. Oxtoby, Phys. Rev. E **62**, 7486 (2000).
[37] R. M. Nyquist, V. Talanquer, and D. W. Oxtoby, J. Chem. Phys. **103**, 1175 (1995).
[38] J. Julin, I. Napari, J. Merikanto, and H. Vehkamäki, J. Chem. Phys. **129**, 234506 (2008).
[39] K. Laasonen, S. Wonczak, R. Strey, and A. Laaksonen, J. Chem. Phys. **113**, 9741 (2000).
[40] J. Wedekind, J. Wölk, D. Reguera, and R. Strey, J. Chem. Phys. **127**, 154515 (2007).
[41] G. Chkonia, J. Wölk, R. Strey, J. Wedekind, and D. Reguera, J. Chem. Phys. **130**, 064505 (2009).
[42] J. Julin, I. Napari, and H. Vehkamäki, J. Chem. Phys. **126**, 224517 (2007).
[43] M. Horsch and J. Vrabec, J. Chem. Phys. **131**, 184104 (2009).
[44] J. Wedekind, G. Chkonia, J. Wölk, R. Strey, and D. Reguera, J. Chem. Phys. **131**, 114506 (2009).
[45] J. L. Lee, J. A. Barker, and F. F. Abraham, J. Chem. Phys. **58**, 3166 (1973).
[46] B. N. Hale and R. C. Ward, J. Stat. Phys. **28**, 487 (1982).
[47] B. N. Hale, Aust. J. Phys. **49**, 425 (1996).
[48] A. V. Neimark and A. Vishnyakov, J. Chem. Phys. **122**, 174508 (2005).
[49] A. V. Neimark and A. Vishnyakov, J. Phys. Chem. B **109**, 5962 (2005).
[50] A. Lauri, J. Merikanto, E. Zapadinsky, and H. Vehkamäki, Atmos. Res. **82**, 489 (2006).
[51] H. Vehkamäki and I. J. Ford, J. Chem. Phys. **112**, 4193 (2000).
[52] J. Merikanto, E. Zapadinsky, A. Lauri, and H. Vehkamäki, Phys. Rev. Lett. **98**, 145702 (2007).
[53] P. R. ten Wolde and D. Frenkel, J. Chem. Phys. **109**, 9901 (1998).
[54] I. Kusaka and D. W. Oxtoby, J. Chem. Phys. **110**, 5249 (1999).
[55] K. J. Oh and X. C. Zeng, J. Chem. Phys. **112**, 294 (2000).
[56] B. Chen, J. I. Siepmann, K. J. Oh, and M. L. Klein, J. Chem. Phys. **115**, 10903 (2001).
[57] B. J. C. Wu, P. P. Wegener, and G. D. Stein, J. Chem. Phys. **69**, 1776 (1978).
[58] R. A. Zahoransky, J. Höschele, and J. Steinwandel, J. Chem. Phys. **103**, 9038 (1995).
[59] R. A. Zahoransky, J. Höschele, and J. Steinwandel, J. Chem. Phys. **110**, 8842 (1999).
[60] A. Fladerer and R. Strey, J. Chem. Phys. **124**, 164710 (2006).
[61] K. Iland, J. Wölk, R. Strey, and D. Kashchiev, J. Chem. Phys. **127**, 154506 (2007).
[62] S. Sinha, A. Bhabhe, H. Laksmono, J. Wölk, R. Strey, and B. Wyslouzil, J. Chem. Phys. **132**, 064304 (2010).
[63] M. Iwamatsu, Chin. J. Phys. (Taipei) **33**, 139 (1995).
[64] J. Barrett, J. Chem. Phys. **111**, 5938 (1999).
[65] G. Wilemski and J.-S. Li, J. Chem. Phys. **121**, 7821 (2004).

[66] S. M. Kathmann, G. K. Schenter, and B. C. Garrett, J. Chem. Phys. **116**, 5046 (2002).
[67] S. M. Kathmann, G. K. Schenter, and B. C. Garrett, J. Chem. Phys. **120**, 9133 (2004).
[68] J. Merikanto, H. Vehkamäki, and E. Zapadinsky, J. Chem. Phys. **121**, 914 (2004).
[69] B. Chen, J. I. Siepmann, and M. L. Klein, J. Phys. Chem. A **109**, 1137 (2005).
[70] I. E. Parra and J. C. Graña, J. Chem. Phys. **132**, 034702 (2010).
[71] B. Smit, J. Chem. Phys. **96**, 8639 (1992).
[72] *Fundamentals of Inhomogeneous Fluids*, edited by D. Henderson (Marcel Dekker, New York, 1992).
[73] A. Laaksonen, V. Talanquer, and D. W. Oxtoby, Annu. Rev. Phys. Chem. **46**, 489 (1995).
[74] N. F. Carnahan and K. E. Starling, J. Chem. Phys. **51**, 635 (1969).
[75] J. D. Weeks, D. Chandler, and H. C. Andersen, J. Chem. Phys. **54**, 5237 (1971).
[76] B. Lu, R. Evans, and M. M. Telo da Gama, Mol. Phys. **55**, 1319 (1985).
[77] B. Chen, J. I. Siepmann, K. J. Oh, and M. L. Klein, J. Chem. Phys. **116**, 4317 (2002).
[78] S. M. Kathmann, G. K. Schenter, B. C. Garrett, B. Chen, and J. I. Siepmann, J. Phys. Chem. C **113**, 10354 (2009).
[79] J. J. Potoff and A. Z. Panagiotopoulos, J. Chem. Phys. **109**, 10914 (1998).
[80] National Institute of Standards and Technology Chemistry Webbook, http://webbook.nist.gov/chemistry/.
[81] A. A. Abrahamson, Phys. Rev. **130**, 693 (1963).
[82] E. A. Mason and W. E. Rice, J. Chem. Phys. **22**, 843 (1954).
[83] R. J. Sadus and J. M. Prausnitz, J. Chem. Phys. **104**, 4784 (1996).
[84] G. Marcelli and R. J. Sadus, J. Chem. Phys. **111**, 1533 (1999).
[85] J. A. Barker, R. A. Fisher, and R. O. Watts, Mol. Phys. **21**, 657 (1971).
[86] A. E. Nasrabad and R. Laghaei, J. Chem. Phys. **125**, 084510 (2006).
[87] A. E. Nasrabad, J. Chem. Phys. **129**, 244504 (2008).
[88] M. Mecke, J. Winkelmann, and J. Fischer, J. Chem. Phys. **107**, 9264 (1997).
[89] B. Chen, H. Kim, S. J. Keasler, and R. B. Nellas, J. Phys. Chem. B **112**, 4067 (2008).
[90] E. Salomons and M. Mareschal, J. Phys.: Condens. Matter **3**, 3645 (1991).
[91] A. Z. Panagiotopoulos, Mol. Phys. **61**, 813 (1987).
[92] A. Z. Panagiotopoulos, N. Quirke, M. Stapleton, and D. J. Tildesley, Mol. Phys. **63**, 527 (1988).
[93] B. Smit and D. Frenkel, Mol. Phys. **68**, 951 (1989).
[94] D. Frenkel and B. Smit, *Understanding Molecular Simulation: From Algorithms to Applications* (Academic, London, 2002).
[95] J. I. Siepmann, I. R. McDonald, and D. Frenkel, J. Phys.: Condens. Matter **4**, 679 (1992).
[96] M. G. Martin and J. I. Siepmann, Theor. Chem. Acc. **99**, 347 (1998).
[97] B. Chen and J. I. Siepmann, J. Phys. Chem. B **104**, 8725 (2000).
[98] B. Chen and J. Ilja Siepmann, J. Phys. Chem. B **105**, 11275 (2001).
[99] F. H. Stillinger, Jr., J. Chem. Phys. **38**, 1486 (1963).
[100] J. I. Siepmann and D. Frenkel, Mol. Phys. **75**, 59 (1992).
[101] N. B. Wilding, Phys. Rev. E **52**, 602 (1995).
[102] G. M. Torrie and J. P. Valleau, Chem. Phys. Lett. **28**, 578 (1974).
[103] J. R. Errington and A. Z. Panagiotopoulos, J. Chem. Phys. **109**, 1093 (1998).
[104] N. T. Tsona, "Monte Carlo simulation of the homogeneous vapor-liquid nucleation of some rare gases," M.S. thesis, University of Dschang, Cameroon, 2008.
[105] J.-P. Hansen and I. R. McDonald, *Theory of Simple Liquids*, 3rd ed. (Elsevier, San Diego, 2006).